energies

MDPI

Article

Improvement of Fuzzy Newton Power Flow Convergence

Ligang Zhao [1], Hua Zheng [2,*], Hongyue Zhen [1], Li Xie [2], Yuan Xu [1] and Xianchao Huang [2]

[1] CSG Electric Power Research Institute China Southern Power Grid, Guangzhou 510663, China; zhaolg@csg.cn (L.Z.); zhenhy@csg.cn (H.Z.); xuyuan@csg.cn (Y.X.)
[2] School of Electrical & Electronic Engineering, North China Electric Power University, Beijing 102206, China; dht_tony@163.com (L.X.); hxc241@163.com (X.H.)
* Correspondence: zhenghua@ncepu.edu.cn

Abstract: In order to address the convergence issue in fuzzy power flow calculations, this paper proposes an analytical approach based on the Levenberg–Marquardt method, aiming to improve the convergence of the fuzzy Newton power flow method. Firstly, a detailed analysis is conducted on the convergence theorem and convergence behavior of the fuzzy Newton method, revealing its poor convergence when the initial values are not properly selected. The Levenberg–Marquardt method is then selected as a means to enhance the convergence of the fuzzy Newton power flow calculations, specifically to tackle the problem of initial value deviation. Since the Jacobian matrix has a significant impact on the convergence region of the power flow, this paper reconstructs the Jacobian matrix based on the Levenberg–Marquardt method, effectively enlarging the convergence region. Through validation experiments on the IEEE 118 standard nodes and simulation comparative analysis, the results confirm the method's effectiveness in resolving the problem of initial value deviation and notably enlarging the convergence region, thereby improving the convergence of power flow calculations.

Keywords: Levenberg–Marquardt; power flow calculation; convergence; fuzzy-Newton method

Citation: Zhao, L.; Zheng, H.; Zhen, H.; Xie, L.; Xu, Y.; Huang, X. Improvement of Fuzzy Newton Power Flow Convergence. *Energies* **2023**, *16*, 8044. https://doi.org/10.3390/en16248044

Academic Editor: José Gabriel Oliveira Pinto

Received: 4 November 2023
Revised: 29 November 2023
Accepted: 5 December 2023
Published: 13 December 2023

1. Introduction

There are numerous variables of uncertainty in power systems [1,2], which are typically handled as planning and forecasting problems. Power systems involve more complex analyses, such as load flow [3–5], and using deterministic methods for analysis cannot provide accurate results. Borkowska [6] introduced the concept of probabilistic flow, which is applied to the DC model. The injection power of uncertain nodes is modeled using probability functions. Subsequently, the probability functions are applied to the AC model, initiating numerical analysis [7]. When analyzing probabilistic flow, boundary flow analysis [8] is conducted to evaluate the maximum and minimum values that flow state variables can assume.

However, there are still many uncertain variables in power systems that can be considered as non-probabilistic in certain operating conditions. The magnitude of loads is constantly changing at any given moment due to economic growth, changes in social conditions, and human behavior. Therefore, in some cases, using past experience to evaluate future events is an incomplete approach. On the contrary, uncertainty in actual power systems is often associated with imprecise qualitative information and is also linked to certain common expressions, such as "rated power of the motor is between 15 and 25 MW" or "negative power is approximately 5 MW", which are typically derived from the experience of system operators. Uncertainty analysis of existing models is necessary when non-probabilistic uncertainties arise in the power system [9]. Fuzzy sets are commonly used for analysis as they can represent and analyze variables with fuzzy and imprecise mathematical precision. Miranda and Mato proposed fuzzy power flow calculation [10–13] to study fuzzy variables in power system flows, aiming to compute the uncertainties in

power flows by utilizing fuzzy membership functions for node injection powers and addressing potential distribution issues. The possibility analysis model introduced in power flow calculations has been widely accepted. In [14], the fuzzy interval algorithm [15–19] is used to solve power flow calculation problems. Although it is a fuzzy model in specific cases, it represents an alternative way to handle uncertain boundaries. It paves the way for new probabilistic power flow solutions, where this method requires imprecise and fuzzy information as input variables instead of probability density functions.

Fuzzy power flow has been widely applied in the operation and planning of power systems since its proposal, including power transmission systems [20,21], distribution networks, and distributed generation systems [22–25]. This has led to new requirements for fuzzy power flow algorithms. Consequently, over time, traditional fuzzy power flow algorithms have undergone changes. In [26], improvements to the power flow calculation method were made based on numerical values such as branch losses, voltage, and current between nodes. Although there are many traditional applications, their use in large-scale systems is limited. This paper aims to improve the traditional fuzzy power flow algorithm to make it suitable for large-scale power transmission systems. Research on power flow calculation has a long history, and there is already a certain foundation in studying the convergence of power flow calculation, especially the convergence issue of the Newton method for power flow calculation, which has been favored by researchers. In order to address the sensitivity of the Newton method to the selection of initial values, in [27], the authors propose using the PO decoupling method for 1–2 iterations and using the updated solution as the initial value to start the Newton iteration, which has achieved good results. The power flow module in the PSD-BPA (2.9) software of the Electric Power Research Institute still retains this option. In [28], the authors replace the node admittance with the injected power as the elements of the Jacobian matrix and improve the convergence of power flow when calculating nodes with large loads by enlarging the smallest eigenvalue of the Jacobian matrix. Another group of algorithms takes a different approach. In [29], the elimination tree theory for power flow calculation is proposed. This method does not involve inverting the admittance matrix, thus avoiding convergence issues. However, current power system networks are generally complex with a large number of nodes, which increases the computational burden and slows down computer performance when applying this method to complex power networks, making it difficult to improve convergence. In [30], a power flow calculation method based on adjoint theory is proposed, which uses numerical integration to solve the power flow equations and constructs a least squares formulation. This method has achieved certain results in challenging-to-converge small systems.

The Levenberg–Marquardt (LM) method is an iterative algorithm for solving nonlinear least squares problems. It combines the features of the most rapid descent method with the Gauss–Newton method and aims to find the parameter that minimizes the sum of squares of the residuals between the predicted and observed values of the model. In [31], they first applied the LM method to power flow calculations, and through numerical simulations, it was demonstrated that the LM method expanded the range of initial value selection for power flow convergence. In the Levenberg–Marquardt method, it is first necessary to define an objective function and transform the fitting problem into a problem of minimizing the objective function. The algorithm then progressively updates the parameters by iterating to minimize the objective function. During each iteration, the gradient of the objective function under the current parameters, i.e., the partial derivative of the loss function with respect to each parameter, is first calculated. Then, based on the current gradient and previous iteration information, a new parameter update direction is calculated. Then, based on this update direction, a new parameter value is computed and used to update the model. The main feature of the Levenberg–Marquardt method is that in each iteration, the Hessian matrix of the objective function is multiplied by a positive definite matrix to obtain a more accurate parameter update direction. The parameters of this positive definite matrix are adjusted in each iteration to control the step size and direction of the model update.

The above references analyze the improvement of convergence for traditional Newton power flow calculation methods in conventional power grids. This paper will be based on the Levenberg–Marquardt method, focusing on the energy interconnection system, to study methods to improve the convergence of fuzzy Newton method power flow algorithms.

In this paper, by analyzing the convergence theorem and convergence tendency of the fuzzy Newton tidal current algorithm and combining it with existing methods to improve the convergence of the tidal current calculation, we propose an analytical method to improve the convergence of the fuzzy Newton tidal current calculation based on the Levenberg–Marquardt method, which reduces the number of iterations and the running time of the tidal current calculation and expands the convergence region. This method reduces the number of iterations and the running time of the tidal current calculation and enlarges the convergence region. In conclusion, the analytical method to improve the convergence of the fuzzy Newton method based on the Levenberg–Marquardt algorithm proposed in this paper has important theoretical significance and practical value. It provides a new and effective tidal current calculation method in the field of power system analysis, which helps to improve the stability and operation efficiency of the power system.

The rest of the paper is organized as follows: In Section 2, the fuzzy set theory is applied to construct a fuzzy tidal current model for the generating units of the power system. Subsequently, in Section 3, the convergence problem of fuzzy current calculation is investigated, and it is shown that the Jacobian matrix is an important factor affecting the convergence of the current. And we analyze the convergence of the fuzzy tidal current calculation method and propose corresponding methods to improve the convergence. In Section 4, we use the Levenberg–Marquardt method applied to the fuzzy tidal current calculation. Given the content of the previous analysis, it is known that the influence of the Jacobian matrix on the convergence of the tidal current calculation is huge. In order to improve the convergence of the tidal currents, we reconstruct the Jacobian matrix based on this method. Finally, the simulation results show that our method reduces the number of calculation iterations and expands the convergence region, which verifies that our proposed method is effective.

2. Fuzzy Modeling of the Uncertainty in the Output and Availability of Power Generation Device

In this paper, the fuzzy modeling of the power generation unit is achieved using the trapezoidal fuzzy number. The estimates of the power generation unit appear between $L_1 \sim L_4$, but most likely between $L_2 \sim L_3$, and the uncertainty of the power generation unit is described through the affiliation function by using the following trapezoidal fuzzy number $\widetilde{L} = (L_1, L_2, L_3, L_4)$.

$$\mu_{\widetilde{L}}(x) = \begin{cases} 0 & x < L_1 \\ \frac{x-L_1}{L_2-L_1} & L_1 \le x < L_2 \\ 1 & L_2 \le x < L_3 \\ \frac{x-L_1}{L_2-L_1} & L_3 \le x < L_4 \\ 0 & x \ge L_4 \end{cases} \tag{1}$$

The fuzzy number center value is $\mu_{\widetilde{L}}(x) = 1$ The mean of the intercept is $\frac{L_2+L_3}{2}$.

The fuzzy availability of the kth generator at the ith node is denoted by $\widetilde{A}_{G_{ik}}$, the active fuzzy output and fuzzy load are denoted by $\widetilde{P}_{G_{ik}}$, $\widetilde{P}_{L_i}$, and the reactive fuzzy output and

fuzzy load are denoted by an $\widetilde{Q}_{G_{ik}}$ $\widetilde{Q}_{L_i}$, respectively. In this case, the fuzzy active and fuzzy reactive powers injected by the node i can be represented by the following equation:

$$\begin{cases} \widetilde{P}_i = \sum_{k=1}^{n} \widetilde{P}_{G_{ik}} . \widetilde{A}_{G_{ik}} - \widetilde{P}_{L_i} \\ \widetilde{Q}_i = \sum_{k=1}^{n} \widetilde{Q}_{G_{ik}} . \widetilde{A}_{G_{ik}} - \widetilde{Q}_{L_i} \end{cases} \tag{2}$$

In Equation (2), n is the number of power-generating devices on node i. By performing fuzzy number operations on $\widetilde{P}_i$, $\widetilde{Q}_i$, it can be determined that they are trapezoidal fuzzy numbers.

Distributed generation device wind turbine generators are driven by the wind, and the wind blades drive the horizontal or longitudinal axis to rotate. This converts mechanical torque into mechanical energy, and the generator uses the transmission device to obtain mechanical power. The stator induces an electric current via the rotation of the rotor, and the power generated is subsequently transferred to the grid on the stator side.

The wind speed, which conforms to the Weibull distribution, is given by the following equation:

$$\varphi(v) = \frac{k}{c}\left(\frac{v}{c}\right)^{k-1} \exp[-(\frac{v}{c})^k] \tag{3}$$

where $k = 2$ denotes the shape parameter, $c = 7$ m/s denotes the scale parameter, and v is the random variable of the Weibull distribution.

In fuzzy tidal current calculation, the wind speed needs to be fuzzified to derive the fuzzy power emitted by the wind turbine. In order to obtain the fuzzy distribution function of wind power, a probability distribution function is used, which is transformed into a fuzzy distributed function by fuzzifying the wind speed. That is to say, the left and right sides of the maximum value x^m are fuzzified, as are the left side of any value $x' \in [-\infty, x^m]$ and the right side of any value $x'' \in [x^m, +\infty]$:

$$P(x') = P(x'') = \int_{-\infty}^{x'} p(y)dy + \int_{x''}^{+\infty} p(y)dy \tag{4}$$

where $P(x')$ is the fuzzy affiliation function.

Nodes with loads in energy interconnection systems usually have transformers connected to them. Generally, the size of the load is related to the capacity of the connected transformer, since the size of the load of the node will not be lower than 20% or higher than 120% of the capacity of the transformer, but normally varies from 60% to 80% of the capacity of the transformer. So, the magnitude of the node load is described by a set of fuzzy interval numbers corresponding to the determination intervals $\left[{\beta^1}_{xi}, {\beta^r}_{xi}\right]$ and $\left[{\alpha^1}_{xi}, {\alpha^r}_{xi}\right]$. $\left\{{\beta^1}_{xi}, {\beta^r}_{xi}, {\alpha^1}_{xi}, {\alpha^r}_{xi}\right\}$, where ${\beta^1}_{xi} = 0.6x_{Ni}, {\beta^r}_{xi} = 0.8x_{Ni}, {\alpha^1}_{xi} = 0.2x_{Ni}, {\alpha^r}_{xi} = 1.2x_{Ni}$, where the rated values of active power P and reactive power Q (denoted by x) at node i of ab are denoted by x_{Ni}.

The affiliation function is shown below:

$$\mu_{x_i} \begin{cases} \frac{x_i - {\alpha^1}_{xi}}{{\beta^1}_{xi} - {\alpha^1}_{xi}} & {\alpha^1}_{xi} \le x_i \le {\beta^1}_{xi} \\ \frac{x_i - {\alpha^r}_{xi}}{{\beta^r}_{xi} - {\alpha^r}_{xi}} & {\beta^r}_{xi} \le x_i \le {\alpha^r}_{xi} \\ 1 & {\beta^1}_{xi} \le x_i \le {\beta^r}_{xi} \\ 0 & else \end{cases} \tag{5}$$

where x stands for P or Q.

For the electric vehicle charging pile load in the energy interconnection system, assuming that it can run continuously from entering the operation state to exiting, the number of fuzzy intervals that determines the boundary [0, Q_{Gmax}] or with uncertainty

$\{0, 0, Q_{Gmax}, Q_{Gmax}\}$ can describe the operation process, where Q_{Gmax} denotes the maximum capacity of the charger.

For the industrial loads of an electric arc furnace and aluminum electrolysis in the energy interconnection system, its fuzzy interval model $\{0, 0, Q_{Gmax}, Q_{Gmax}\}$ can be obtained using the same method, where Q_{Gmax} denotes the maximal capacity of an electric arc furnace and aluminum electrolysis. When the variables of the energy interconnection system are in the fuzzy interval $\left[\beta^1{}_{xi}, \beta^r{}_{xi}\right]$, $\alpha^1{}_{xi} = \beta^1{}_{xi}$, $\alpha^r{}_{xi} = \beta^r{}_{xi}$, and the subordination value of the variables is 1, the fuzzy trend calculation is changed to the deterministic trend calculation; when $\beta^1{}_{xi} = \beta^r{}_{xi}$, the fuzzy trend calculation is changed to the triangular fuzzy number; when $\beta^1{}_{xi} = \beta^r{}_{xi}$, it becomes the triangular fuzzy number. When $\alpha^1{}_{xi} = \beta^1{}_{xi} = \alpha^r{}_{xi} = \beta^r{}_{xi}$, it becomes the traditional Newtonian tidal current calculation.

3. Convergence Analysis of the Fuzzy Newton Method

Since the convergence of Newton's method is mainly related to the Jacobian matrix, to analyze the convergence of the fuzzy Newton's method, the Jacobian matrix has to satisfy the following conditions.

Assumption 1. *The Jacobian matrix J_k satisfies the Lipschitz condition after the kth Newton's method of selecting generations:*

$$\| J_m - J_n \| \leq \gamma \| V_m - V_n \|, \forall V_m, V_n \in S(V_0, \delta) \tag{6}$$

where γ is a real number.

Lemma 1. *Let $A, C \in L(R^n)$. A is a non-singular matrix; $\| A^{-1} \| \leq \alpha$, $\| A - C \| \leq \beta$ and $\alpha\beta < 1$, then*

$$\| C^{-1} \| \leq \frac{\alpha}{1 - \alpha\beta} \tag{7}$$

Theorem 1. *The initial value of voltage V_0 and the Jacobian matrix J_k in the fuzzy trend calculation $\widetilde{F}(V) = 0$ satisfy the following conditions:*

$$\| J_0{}^{-1} \| \leq \beta \tag{8}$$

$$\| J_0{}^{-1} \widetilde{F}(V) \| \leq \eta \tag{9}$$

where β, η are real numbers. In the neighborhood $S(V_0, \delta)$ of the voltage magnitude V_0, if the fuzzy tidal current calculation convergence operator ρ satisfies the following conditions:

$$\rho = \beta\eta\gamma \leq \frac{1}{2} \tag{10}$$

$$\delta \geq \frac{1 - \sqrt{1 - 2\rho}}{\rho}\eta \tag{11}$$

The solution sequence V_k of the fuzzy Newton method for power flow calculation converges at V^*, indicating the existence of a solution V^* within the range of $S(V_0, \delta)$.

Proof of Theorem 1. From the quadratic merit function, we get:

$$j(x) = \frac{1}{2}\gamma x^2 - \frac{1}{\beta}x + \frac{\eta}{\beta} = 0 \tag{12}$$

The two analytical solutions can be obtained as $\tilde{x}^{*} = \frac{1-\sqrt{1-2\beta\gamma\eta}}{\beta\gamma}$, $\tilde{x}^{**} = \frac{1+\sqrt{1-2\beta\gamma\eta}}{\beta\gamma}$, which is carried into the Equation (10) and the Equation (11) to get:

$$\tilde{x}^{*} = \frac{1-\sqrt{1-2\rho}}{\rho}\eta,\ \tilde{x}^{**} = \frac{1+\sqrt{1-2\rho}}{\rho}\eta \tag{13}$$

The iterative sequence $x_{k+1} = x_k - \frac{j(x_k)}{j'(x_k)}$, $k = 0, 1, 2, \cdots$, $x_0 = 0$ is denoted by t_k, which confirms that $x_k \to x^*$. Next, we analyze $\| \Delta V_k - \Delta V^* \| \leq x^* - x_k$.

Let $\eta_k = x_{k+1} - x_k = -\frac{j(x_k)}{j'(x_k)}$, $\beta_k = -\frac{1}{j'(x_k)}$, $\rho_k = \beta_k\gamma_k\eta$, when $k = 0$, $\eta_0 = \eta$, $\beta_0 = \beta$. Derivation of Equation (11), we get:

$$j\prime(x) = \gamma x - 1/\beta \tag{14}$$

we substitute the $j\prime(x_{k+1})$ and $j'(x_k)$ into Equations (13) and (14), and we get:

$$j'(x_{k+1}) - j'(x_k) = \gamma(x_{k+1} - x_k) = \gamma\eta_k \tag{15}$$

Then, we construct a function of the following form:

$$\begin{aligned} & j(x_{k+1}) - [j(x_k) + j'(x_k)(x_{k+1} - x_k)] \\ &= \tfrac{1}{2}\gamma {x^2}_{k+1} - \tfrac{1}{\beta}x_{k+1} - \tfrac{1}{2}\,\gamma {x^2}_k + \tfrac{1}{\beta}x_k - \left(\gamma x_k - \tfrac{1}{\beta}\right)(x_{k+1} - x_k) \\ &= \tfrac{1}{2}\gamma {x^2}_{k+1} - \tfrac{1}{2}\,\gamma {x^2}_k\left(\gamma x_k - \tfrac{1}{\beta}\right)(x_{k+1} - x_k) \\ &= \tfrac{1}{2}\gamma\eta_k(x_{k+1} - x_k) - \left(\gamma x_k - \tfrac{1}{\beta}\right)\eta_k \\ &= \tfrac{1}{2}\gamma(x_{k+1} - x_k)^2 = \tfrac{1}{2}\gamma {\eta_k}^2 \end{aligned} \tag{16}$$

From Equation (15), we have:

$$j'(x_{k+1}) = \gamma\eta_k + j'(x_k) = \gamma\eta_k - \frac{1}{\beta_k} = \frac{\gamma\eta_k\beta_k - 1}{\beta_k} = \frac{\rho_k - 1}{\beta_k} \tag{17}$$

Substituting the variables $\beta_k = -\frac{1}{j'(x_k)}$, $\rho_k = \beta_k\gamma_k\eta$ into Equations (16) and (17) yields:

$$\beta_{k+1} = -\frac{1}{j'(x_{k+1})} \tag{18}$$

$$\eta_{k+1} = -\frac{j(x_{k+1})}{j'(x_{k+1})} = \frac{1}{2}\frac{\gamma\beta_k {\eta_k}^2}{1-\rho_k} = \frac{1}{2}\frac{\rho_k}{1-\rho_k}\eta_k \tag{19}$$

$$\rho_{k+1} = \gamma\beta_{k+1}\eta_{k+1} = \frac{\gamma\beta_k}{1-\rho_k}\cdot\frac{\rho_k\eta_k}{2(1-\rho_k)} = \frac{{\rho_k}^2}{2(1-\rho_k)^2} \tag{20}$$

Noting that $0 \leq \rho \leq \frac{1}{2}$, $1 \leq \frac{1-\sqrt{1-2\rho}}{\rho} \leq 2$, there are:

$$\| \Delta V_1 - \Delta V_0 \| = \| [j_0]^{-1} \| \leq \eta_0 = \eta = x_1 - x_0 \tag{21}$$

From (6), (16), (21) and $V^{(1)} \in S\left(V^{(0)}, \delta\right)$ we find that:

$$\| \widetilde{F}\left(V^{(1)}\right) \| = \| \widetilde{F}\left(V^{(1)}\right) - \widetilde{F}\left(V^{(0)}\right) - \widetilde{F}'(v)(V^{(1)} - V^{(0)}) \| \leq \frac{1}{2}\gamma \| V^{(1)} - V^{(0)} \|^2 \leq \frac{1}{2}\gamma {\eta_0}^2 \tag{22}$$

$$v \in \left(V^{(0)}, V^{(1)}\right)$$

$$\| j_1 - j_0 \| \leq \gamma \| V_1 - V_0 \| \leq \gamma\eta_0 \tag{23}$$

Due to $\| j_1{}^{-1} \| \leq \beta$ and $\| j_1 - j_0 \| \leq \gamma \| V_1 - V_0 \| \leq \gamma\eta_0$. Based on Lemma 1, it follows that $j_1{}^{-1}$ exists and that

$$\| j_1{}^{-1} \| \leq \frac{\beta_0}{1-\rho_0} = \beta_1 \tag{24}$$

Since the magnitude of the voltage amplitude is changing as the iteration proceeds, it is important to note what $V^{(1)}$ represents, as shown by Equations (10), (11), and (21).

$$\begin{array}{c} \left\| V^{(2)} - V^{(1)} \right\| \leq x_2 - x_1 = \eta_1 \\ \leq \left(\frac{1-\sqrt{1-2\rho}}{\rho} - 1 \right)\eta + \eta = \frac{1-\sqrt{1-2\rho}}{\rho}\eta \end{array} \tag{25}$$

$$\begin{array}{c} \left\| V^{(2)} - V^{(0)} \right\| \leq \left\| V^{(2)} - V^{(1)} \right\| + \left\| V^{(1)} - V^{(0)} \right\| \leq \\ \left(\frac{1-\sqrt{1-2\rho}}{\rho} - 1 \right)\eta + \eta = \frac{1-\sqrt{1-2\rho}}{\rho}\eta \leq \delta \end{array} \tag{26}$$

The amplitude of the voltage is expressed as $V^{(2)} \in S(V_0, \delta)$.

Similarly to Equations (25) and (26), it follows identically that $V_k \in S(V_0, \delta)$, $k = 0, 1, 2 \ldots$ and we get:

$$\begin{cases} \left\| \widetilde{F}(V_k) \right\| \leq \frac{1}{2}\gamma\eta_{k-1}^2 \\ \left\| J_k^{-1} \right\| \leq \beta_k \\ \left\| J_k^{-1}\widetilde{F}(V_k) \right\| \leq \eta_k \\ \| \Delta V_{k+1} - \Delta V_k \| \leq t_{k+1} - t_k \end{cases} \tag{27}$$

For any positive integers $m,\ n,\ k$, $m = n + k$, we have:

$$\begin{array}{l} \left\| V^{(m)} - V^{(n)} \right\| \leq \left\| V^{(n+k)} - V^{(n+k-1)} \right\| + \cdots + \left\| V^{(k+1)} - V^{(k)} \right\| \\ \leq |x_{n+k} - x_{n+k-1}| + \cdots + |x_{n+1} - x_n| \\ \leq |x_m - x_n| \end{array} \tag{28}$$

It follows from the convergence of t_k that $\{V^{(k)}\}$ is a Cauchy convergent sequence, and thus $\{V^{(k)}\}$ has a limit, which is set to be V^*, so that $k \to \infty$ in the above equation leads to

$$\left\| V^* - V^{(k)} \right\| \leq |x^* - x_k| \tag{29}$$

Observing the convergence of $\eta_k \to 0$ and $\widetilde{F}(V^*)$ through Equation (27), it can be seen that $\widetilde{F}(V^*) = 0$, the solution of the fuzzy tidal current computation $\widetilde{F}(V) = 0$ is V^*, which can end the whole proof of inference process. □

Using this theorem, the difficulty of choosing the initial value is reduced, and fewer computational steps are required to calculate the trend operator ρ before the trend calculation to determine whether the initial value can find a convergent solution for the trend calculation. If ρ is less than $1/2$, the next trend computation can continue; otherwise, it is necessary to repeatedly train other initial values.

4. Levenberg–Marquardt Method Applied to Fuzzy Tidal Current Calculation

4.1. Convergence Improvement Proof

In this paper, the Levenberg–Marquardt method is used to improve the convergence of the fuzzy Newton method of tidal current computation, which belongs to one of the

non-linear least squares computational methods. A first-order *Taylor* expansion of the basic fuzzy tidal current equation $\widetilde{F}(x) = 0$ is performed at the iteration point $x(k)$:

$$\widetilde{F}\left(x^{(k+1)}\right) = \widetilde{F}\left(x^{(k)}\right) + J\left(x^{(k)}\right)\Delta\widetilde{x}^{(k)} \tag{30}$$

where $\Delta\widetilde{x}^{(k)}$ denotes the iterative correction and $\Delta\widetilde{x}^{(k)} = x^{(k+1)} - x^{(k)}$, $x^{(k)} \in \Delta\widetilde{x}^{(k)}$, the least squares of the trending equations are notated:

$$min\widetilde{F}\left(x^{(k+1)}\right) = ||\widetilde{F}\left(x^{(k+1)}\right)||_2^2 \tag{31}$$

We substitute the Equation (30) into Equation (31). Taking a step size of 1/2 for constraints, the computational model for the Levenberg–Marquardt method can be obtained as:

$$min\widetilde{F}(x^{(k+1)}) = \frac{1}{2}||\widetilde{F}(x^{(k)}) + J(x^{(k)})\Delta\widetilde{x}^{(k)}||_2^2 \tag{32}$$

$$||\Delta\widetilde{x}^{(k)}||_2 \leq \delta \tag{33}$$

where δ is a dynamic variable that can be changed according to the demand; to reduce the sum of squares of iterative errors, the magnitude of $\Delta\widetilde{x}^{(k)}$ has to be determined first. Using the Levenberg–Marquardt method to limit the magnitude of iterative corrections by adding a damping factor μ as an additional constraint $\Delta\widetilde{x}^{(k)}$ can be expressed as:

$$\Delta\widetilde{x}^{(k)} = -\left(J\left(\widetilde{x}^{(k)}\right)^T J\left(\widetilde{x}^{(k)}\right) + \mu I\right)^{-1} J\left(\widetilde{x}^{(k)}\right)^T F\left(\widetilde{x}^{(k)}\right) \tag{34}$$

The introduction of the damping factor μ effectively alleviates the divergence problem in the convergence process, and at the same time gives the Levenberg–Marquardt method the following features:

(1) When $\lambda \geq 0$, the number of second-paradigm conditions of the matrix $J^T J + \lambda I$ decreases monotonically as the damping factor μ increases.

Proof. Assuming that the $J^T J$ matrix is an $n \times n$ order matrix with eigenvalues $\lambda_1 \leq \lambda_2 \leq \lambda_3 \cdots \leq \lambda_n$ then for any x, $x^T(J^T J)x = (Jx)^T(Jx) = ||Jx||_2^2 \geq 0$, so the matrix $J^T J$ is a semi-positive definite matrix, and thus all of its eigenvalues can satisfy $0 \leq \lambda_1 \leq \lambda_2 \leq \lambda_3 \cdots \leq \lambda_n$. Therefore, $\lambda_i + \mu \neq 0$. This is because the singular values of a positive definite matrix and the absolute values of its eigenvalues are equal. Since the condition number of the matrix $A = J^T J + \mu I$ is satisfied:

$$cond(A) = \frac{\lambda_n + \mu}{\lambda_1 + \mu} \tag{35}$$

$$[cond(A)]'_\mu = \left(\frac{\lambda_n + \mu}{\lambda_1 + \mu}\right)' = \frac{\lambda_1 - \lambda_n}{(\lambda_1 + \mu)^2} \leq 0 \tag{36}$$

Thus, the second-fan condition number of matrix A decreases monotonically as μ increases. □

(2) The iterative correction $\Delta\widetilde{x}^{(k)}$ for the Levenberg–Marquardt method decreases monotonically with the increase in damping factor μ.

Proof. Due to $(||\Delta\tilde{x}^{(k)}(\mu)||^2)'_\mu = (\Delta\tilde{x}^{(k)})^T(\Delta\tilde{x}^{(k)}(\mu))'_\mu$. The result obtained by taking the derivation of Equation (27) with respect to μ can be obtained:

$$\left(\left|\left|\Delta\tilde{x}^{(k)}(\mu)\right|\right|^2\right)'_\mu = -\left(\Delta\tilde{x}^{(k)}(\mu)\right)^T\left(J\left(x^{(k)}\right)^T J\left(x^{(k)}\right) + \mu I\right)\left(\Delta\tilde{x}^{(k)}(\mu)\right) \tag{37}$$

where $J\left(x^{(k)}\right)^T J\left(x^{(k)}\right) + \mu I$ is a positive–definite matrix, then $(||\Delta\tilde{x}^{(k)}(\mu)||^2)'_\mu < 0$, and $\Delta\tilde{x}^{(k)}$ decreases monotonically as the damping factor μ increases. □

4.2. Convergence Improvement—Reconstructing the Jacobian Matrix

Based on the Levenberg–Marquardt method of improving the fuzzy Newton method of tidal current calculation, the iterative corrections are expressed in the form of (34), which is rewritten in the form of an equation as follows:

$$-\left(J\left(\tilde{x}^{(k)}\right)^T J\left(\tilde{x}^{(k)}\right) + \mu I\right)\Delta\tilde{x}^{(k)} = J\left(\tilde{x}^{(k)}\right)^T F\left(\tilde{x}^{(k)}\right) \tag{38}$$

From the above equation, the matrix $J(\tilde{x}^{(k)})^T J(\tilde{x}^{(k)}) + \mu I$ is rearranged to obtain the same sparse matrix as the conductor matrix, and the sparsification process is carried out according to the following steps:

$$y = J\left(\tilde{x}^{(k)}\right)\Delta\tilde{x}^{(k)}/\beta_k \tag{39}$$

where y is the intermediate variable, $\beta_k = \sqrt{\mu_k}$.

Substituting Equation (39) into Equation (38) yields:

$$\beta_k\Delta\tilde{x}^{(k)} + J\left(\tilde{x}^{(k)}\right)^T y = -J\left(\tilde{x}^{(k)}\right)^T F\left(\tilde{x}^{(k)}\right)/\beta_k \tag{40}$$

Joining Equations (39) and (40) yields the matrix equation shown below:

$$\begin{bmatrix} \beta_k I & J\left(\tilde{x}^{(k)}\right)^T \\ J\left(\tilde{x}^{(k)}\right) & -\beta_k I \end{bmatrix}\begin{bmatrix} \Delta\tilde{x}^{(k)} \\ y \end{bmatrix} = \begin{bmatrix} F\left(\tilde{x}^{(k)}\right) \\ 0 \end{bmatrix} \tag{41}$$

where $F\left(\tilde{x}^{(k)}\right) = -\left(J\left(\tilde{x}^{(k)}\right)^T F\left(\tilde{x}^{(k)}\right)/\beta_k\right.$, and the coefficient matrix of the matrix equation is denoted by A.

The coefficient matrix A of Equation (12) is sparsely reordered, and the sparse coefficient matrix A is as follows:

$$A' = \begin{bmatrix} \begin{bmatrix} \beta_1 I & J_{11}{}^T \\ J_{11} & -\beta_1 I \end{bmatrix} & \begin{bmatrix} 0 & J_{21}{}^T \\ J_{12} & 0 \end{bmatrix} \cdots \begin{bmatrix} 0 & J_{n-1,1}^T \\ J_{1,n-1} & 0 \end{bmatrix} \\ \begin{bmatrix} 0 & J_{12}{}^T \\ J_{21} & 0 \end{bmatrix} & \begin{bmatrix} \beta_2 I & J_{22}{}^T \\ J_{22} & -\beta_2 I \end{bmatrix} \cdots \begin{bmatrix} 0 & J_{n-1,2}^T \\ J_{2,n-1} & 0 \end{bmatrix} \\ \vdots & \vdots \qquad\qquad \vdots \\ \begin{bmatrix} 0 & J_{1,n-1}^T \\ J_{n-1,1} & 0 \end{bmatrix} & \begin{bmatrix} 0 & J_{2,n-1}^T \\ J_{n-1,2} & 0 \end{bmatrix} \cdots \begin{bmatrix} \beta_{n-1} I & J_{n-1,n-1}^T \\ J_{n-1,n-1} & -\beta_{n-1} I \end{bmatrix} \end{bmatrix} \tag{42}$$

where the chunking matrix has the same structure as the conductivity matrix. Figure 1 shows the coefficient matrix sparse rearrangement undirected graph. The corresponding undirected graph of the system's conductivity matrix is M_1, M_2 has the same structure as

M_1, and the associated nodes of M_2 and M_1 are connected to obtain the topology graph denoted as M_3, which is described by M_3, which also describes the coefficient matrix A.

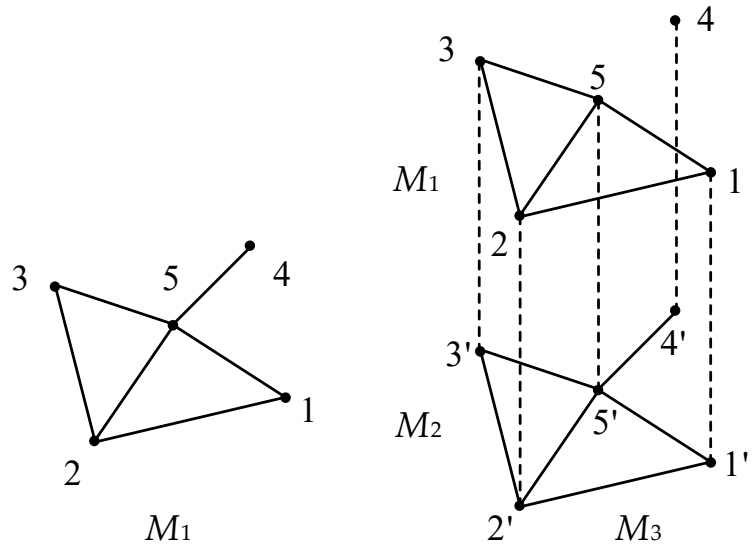

Figure 1. Coefficient matrix sparse rearrangement undirected map.

M_2 has the same structure as M_1, and the nodes of M_3 can be regarded as the generalized nodes of the associated nodes M_1 and M_2. Therefore, the structure of M_3 is the same as that of M_1, so the node ordering of M_1 applies to M_3 as well.

5. Simulation Studies

In this paper, an algorithm for improving the convergence of the fuzzy Newton method of tidal current computation based on the Levenberg–Marquardt method is validated by means of the IEEE 118 standard node system. Figure 2 illustrates the IEEE 118 node structure. The generating unit nodes in this system are 1, 6, 10, 25, 26, 38, 69, 72, 89, 91, 105, 107, 112, 116, etc., and load unit nodes are 16, 45, 47, 58, 70, 85, etc. Where P type nodes are 72, 91; Q type nodes are 25, 116; V type nodes are 38; PQ type nodes are 1, 16, 47, 58; PV type nodes are 10, 26, 89, 105; QV type nodes are 70, 85; $V\theta$ type nodes are 69; and PQV type nodes are 6, 45, 107, 112.

This paper analyzes the convergence of the tidal current calculation based on the initial values of voltage and phase angle of the nodes and the convergence factor K given in the following formula. When K = 1, it means that the convergence has been achieved and there is no need for additional iterations, and when K = 0, it is equivalent to the initialization of all the unknown voltages to 1. In addition, it should be noted that the fuzzy tidal current calculation cannot be converged normally outside the range of a certain convergence factor K.

$$|V_{initial}| = \left|V_{converged}\right|^{K} \tag{43}$$

$$\theta_{initial} = K \times \theta_{converged} \tag{44}$$

There are many methods in the literature for determining the damping factor μ. The Levenberg–Marquardt method for determining the damping factor has a wide range of usability, and it is generally accepted that when the initial value is poorly chosen, it is necessary to choose a larger damping factor μ. In this paper, the damping factor chosen for the simulation varies with the number of iterative corrections, which can be obtained as:

$$\mu = 10^{mlog(\Delta x)+b} \tag{45}$$

where $m = 1$, $b = -3$.

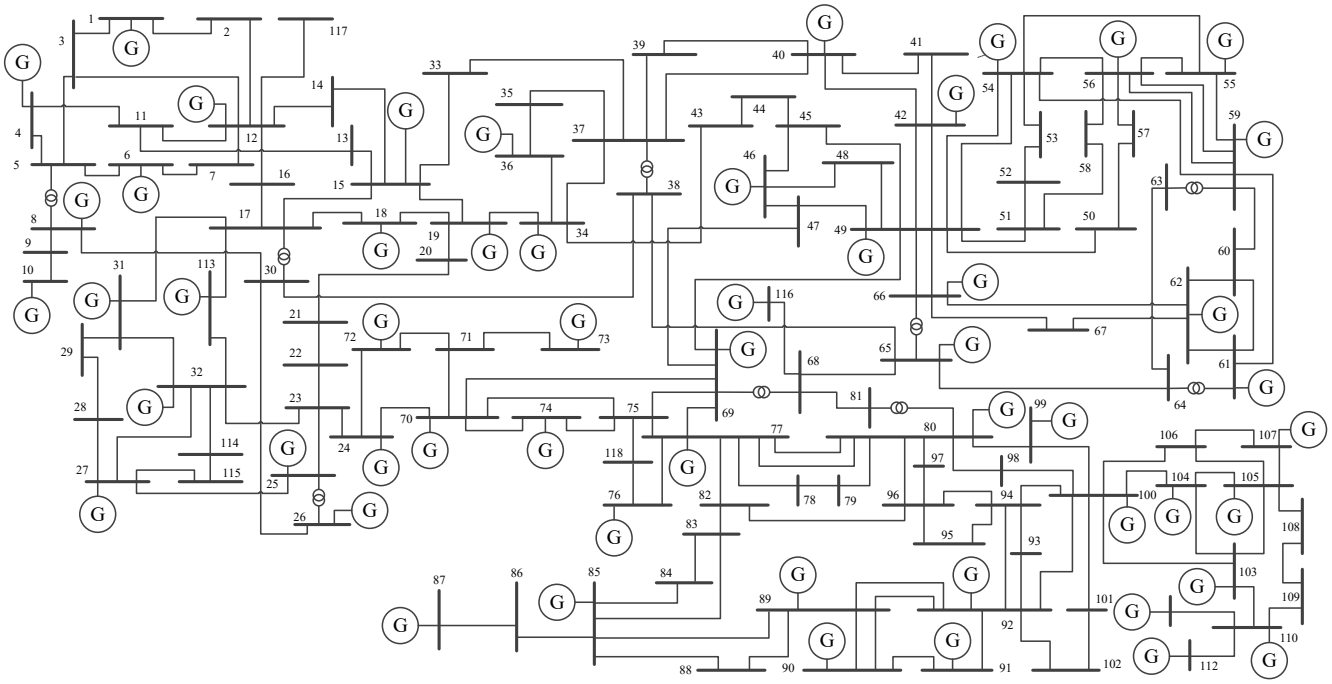

Figure 2. IEEE 118 standard node system.

Figures 3 and 4 depict three different algorithms, namely, the fuzzy Newton method (FNR), the fuzzy Newton method based on the Levenberg–Marquardt method to improve convergence of tidal currents (FNRM), and the fuzzy Newton method based on the Levenberg–Marquardt method to improve convergence of tidal currents after Jacobian matrix reconstruction (FNRMR), with the change in the number of iterations and change in running time graphs, respectively. Algorithms, the number of iterations, and the running time are plotted as the convergence factor changes.

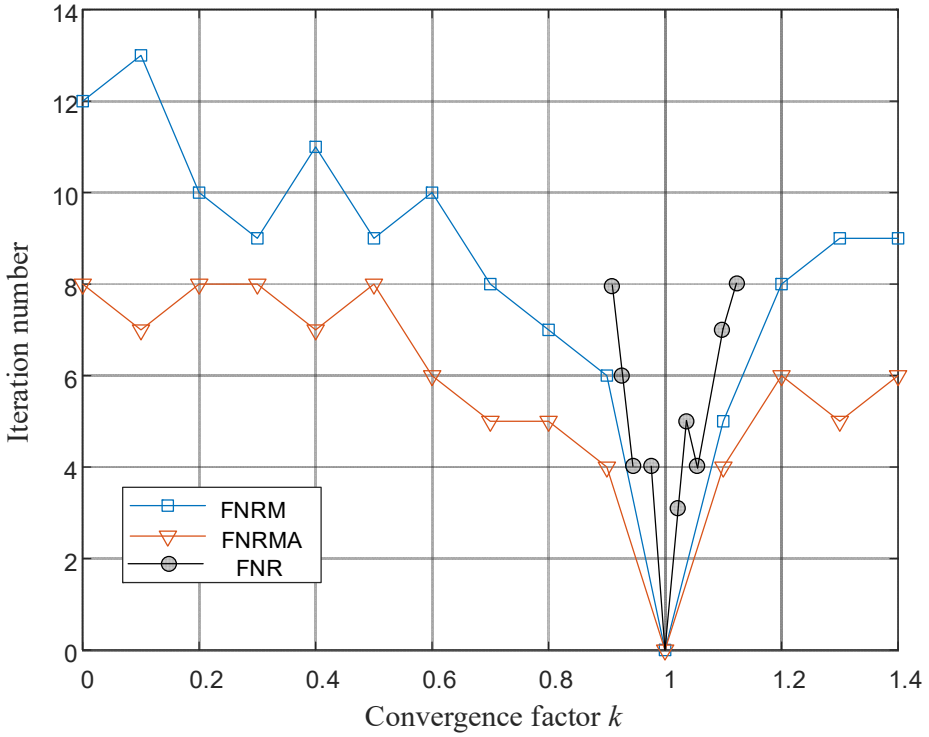

Figure 3. Comparison of the number of iterations with different convergence factors.

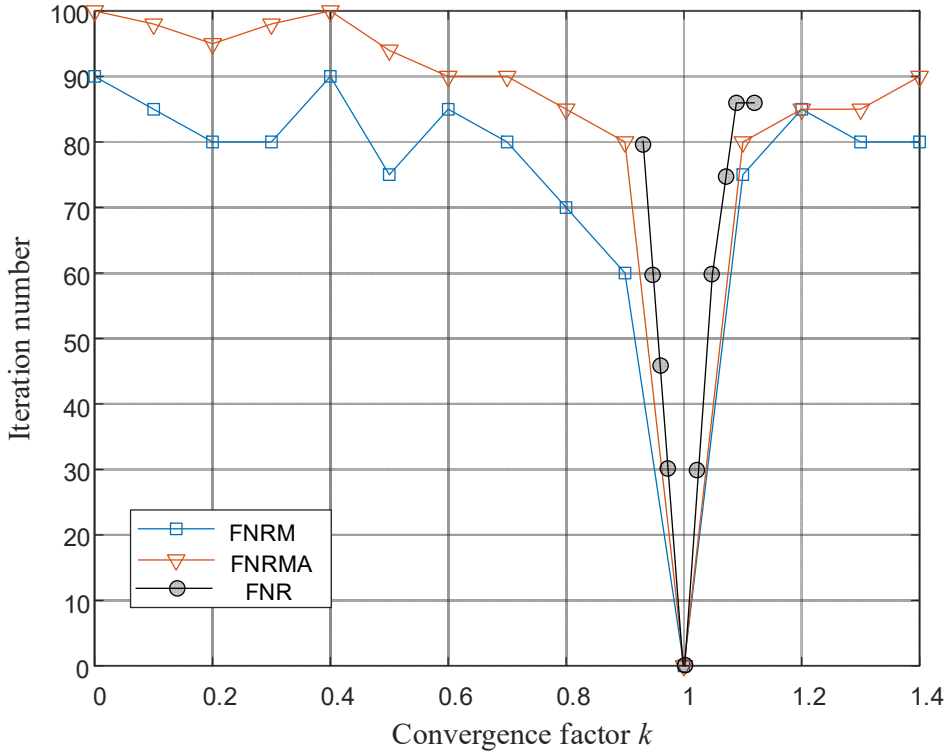

Figure 4. Comparison of running time with different convergence factors.

From the comparative analysis of the above figures, it can be seen that the FNRM and FNRMR methods contain the convergence situation when all unknown voltages are initialized to 1 when $K = 0$. Moreover, the FNRM and FNRMR methods do not need longer iteration times and running times compared with the traditional FNR method, but the convergence region is three times that of the traditional FNR method, and the FNRMR method is able to converge very well even in the case of poorly selected initial values. In addition, the FNRMR method reconstructs the Jacobian matrix through the sparse matrix. Although the process of the sparse matrix increases the running time, the FNRMR significantly reduces the number of iterations, which leads to the conclusion that the fuzzy Newton tidal current algorithm based on the Levenberg–Marquardt algorithm can solve the problem of the deviation of the initial value very well, and expand the convergence region, which improves the tidal current. For the simulation results obtained above, we summarize our advantages from the following two aspects: (1) Number of iterations: Since the fuzzy Newton method with adjusted Jacobian matrix is characterized by dynamically adjusted convergence factors, it can usually approximate the optimal solution faster, and therefore fewer iterations will be required. Meanwhile, the fuzzy Newton method may require more iterations to converge. (2) Running Time: Since the fuzzy Newton method, after adjusting the Jacobian matrix, requires additional computations to update the convergence factors, it may require more running time. However, if the method is able to converge faster, the total running time may be shorter than the fuzzy Newton method. The Levenberg–Marquardt fuzzy Newton tidal current algorithm can solve the problem of initial value deviation well and expand the convergence region to improve the convergence of the tidal current calculation.

6. Conclusions

By analyzing the convergence theorem and convergence tendency of the fuzzy Newton tidal current algorithm and combining them with the existing main methods to improve the convergence of tidal current calculation, an analytical method to improve the convergence of fuzzy Newton tidal current calculation based on the Levenberg–Marquardt method is proposed and verified on the IEEE standard 118 points. The convergence of fuzzy Newton

tidal current calculation, fuzzy Newton tidal current calculation based on Levenberg–Marquardt method, and fuzzy Newton tidal current calculation based on Jacobian matrix reconstruction after the Levenberg–Marquardt method are analyzed by comparison with the simulation. The number of iterations and running time of the fuzzy Newton method, the fuzzy Newton method based on the Levenberg–Marquardt method, and the fuzzy Newton method based on the Levenberg–Marquardt method after the Jacobian matrix reconstruction are compared and analyzed by simulation, and the improved method reduces the number of iterations and enlarges the area of convergence, which verifies that the method can improve the convergence of the fuzzy Newton method.

Author Contributions: Conceptualization, L.Z. and Y.X.; Investigation, L.Z. and X.H.; Methodology, H.Z. (Hua Zheng) and H.Z. (Hongyue Zhen); Resources, H.Z. (Hua Zheng); Software, H.Z. (Hua Zheng) and L.X.; Supervision, H.Z. (Hongyue Zhen); Validation, H.Z. (Hongyue Zhen) and L.X.; Writing-original draft, Y.X.; Writing-review and editing, X.H.; All authors have read and agreed to the published version of the manuscript.

Funding: This work is supported by State Key Laboratory of HVDC.

Data Availability Statement: The data that support the findings of this study are available from the corresponding authors upon reasonable request.

Conflicts of Interest: The authors declare no conflict of interest.

References

1. Maslennikov, V.A.; Ustinov, S.M.; Milanović, J.V. Method for Considering Uncertainties for Robust Tuning of PSS and Evaluation of Stability Limits. *IEE Proc. Gener. Transm. Distrib.* **2002**, *149*, 295–299. [CrossRef]
2. Jordehi, A.R. How to Deal with Uncertainties in Electric Power Systems? A Review. *Renew. Sustain. Energy Rev.* **2018**, *96*, 145–155. [CrossRef]
3. Gianto, R.; Purwoharjono; Imansyah, F.; Kurnianto, R.; Danial. Steady-State Load Flow Model of DFIG Wind Turbine Based on Generator Power Loss Calculation. *Energies* **2023**, *16*, 3640. [CrossRef]
4. Karimi, M.; Shahriari, A.; Aghamohammadi, M.R.; Marzooghi, H.; Terzija, V. Application of Newton-Based Load Flow Methods for Determining Steady-State Condition of Well and Ill-Conditioned Power Systems: A Review. *Int. J. Electr. Power Energy Syst.* **2019**, *113*, 298–309. [CrossRef]
5. Chen, Y.; Wen, J.; Cheng, S. Probabilistic Load Flow Method Based on Nataf Transformation and Latin Hypercube Sampling. *IEEE Trans. Sustain. Energy* **2013**, *4*, 294–301. [CrossRef]
6. Borkowska, B. Probabilistic Load Flow. *IEEE Trans. Power Appar. Syst.* **1974**, *PAS-93*, 752–759. [CrossRef]
7. Sereeter, B.; van Westering, W.; Vuik, C.; Witteveen, C. Linear Power Flow Method Improved with Numerical Analysis Techniques Applied to a Very Large Network. *Energies* **2019**, *12*, 4078. [CrossRef]
8. Dimitrovski, A.; Tomsovic, K. Boundary Load Flow Solutions. *IEEE Trans. Power Syst.* **2004**, *19*, 348–355. [CrossRef]
9. Hakami, A.M.; Hasan, K.N.; Alzubaidi, M.; Datta, M. A Review of Uncertainty Modelling Techniques for Probabilistic Stability Analysis of Renewable-Rich Power Systems. *Energies* **2023**, *16*, 112. [CrossRef]
10. Xu, H.; Yu, Z.; Zheng, Q.; Hou, J.; Wei, Y.; Zhang, Z. Deep Reinforcement Learning-Based Tie-Line Power Adjustment Method for Power System Operation State Calculation. *IEEE Access* **2019**, *7*, 156160–156174. [CrossRef]
11. Singh, V.; Moger, T.; Jena, D. Probabilistic Load Flow for Wind Integrated Power System Considering Node Power Uncertainties and Random Branch Outages. *IEEE Trans. Sustain. Energy* **2023**, *14*, 482–489. [CrossRef]
12. Rejc, M.; Pantos, M. Short-Term Transmission-Loss Forecast for the Slovenian Transmission Power System Based on a Fuzzy-Logic Decision Approach. *IEEE Trans. Power Syst.* **2011**, *26*, 1511–1521. [CrossRef]
13. Wang, Z.; Alvarado, F.L. Interval Arithmetic in Power Flow Analysis. *IEEE Trans. Power Syst.* **1992**, *7*, 1341–1349. [CrossRef] [PubMed]
14. Varshney, A.K.; Mehra, P.; Muhuri, P.K.; Danish Lohani, Q.M. Interval-Valued Fuzzy c-Means Algorithm and Interval-Valued Density-Based Fuzzy c-Means Algorithm. In Proceedings of the 2020 IEEE International Conference on Fuzzy Systems (FUZZ-IEEE), Glasgow, UK, 19–24 July 2020; pp. 1–6. [CrossRef]
15. Luo, M.; Li, W.; Shi, H. The Relationship between Fuzzy Reasoning Methods Based on Intuitionistic Fuzzy Sets and Interval-Valued Fuzzy Sets. *Axioms* **2022**, *11*, 419. [CrossRef]
16. Zeng, S.; Tang, M.; Sun, Q.; Lei, L. Robustness of Interval-Valued Intuitionistic Fuzzy Reasoning Quintuple Implication Method. *IEEE Access* **2022**, *10*, 8328–8338. [CrossRef]
17. Luo, M.; Zhou, X. Interval-Valued Quintuple Implication Principle of Fuzzy Reasoning. *Int. J. Approx. Reason.* **2017**, *84*, 23–32. [CrossRef]
18. Perez, J.; Valdez, F.; Castillo, O.; Melin, P.; Gonzalez, C.; Martinez, G. Interval Type-2 Fuzzy Logic for Dynamic Parameter Adaptation in the Bat Algorithm. *Soft Comput.* **2017**, *21*, 667–685. [CrossRef]

19. Gang, L.; Dongyuan, S.; Jinfu, C.; Xianzhong, D. Automatic Identification of Transmission Sections Based on Complex Network Theory. *IET Gener. Transm. Distrib.* **2014**, *8*, 1203–1210. [CrossRef]
20. Xu, W.; Wang, X.; Li, W.; Li, S.; Lu, C. Research on Test and Evaluation Method of Laser Wireless Power Transmission System. *EURASIP J. Adv. Signal Process.* **2022**, *2022*, 20. [CrossRef]
21. Chen, G.; Lewis, F.L.; Feng, E.N.; Song, Y. Distributed Optimal Active Power Control of Multiple Generation Systems. *IEEE Trans. Ind. Electron.* **2015**, *62*, 7079–7090. [CrossRef]
22. Gu, Q.; Li, S.; Liao, Z. Solving Nonlinear Equation Systems Based on Evolutionary Multitasking with Neighborhood-Based Speciation Differential Evolution. *Expert Syst. Appl.* **2024**, *238*, 122025. [CrossRef]
23. Cao, B.; Dong, W.; Lv, Z.; Gu, Y.; Singh, S.; Kumar, P. Hybrid Microgrid Many-Objective Sizing Optimization with Fuzzy Decision. *IEEE Trans. Fuzzy Syst.* **2020**, *28*, 2702–2710. [CrossRef]
24. Cao, B.; Zhao, J.; Lv, Z.; Gu, Y.; Yang, P.; Halgamuge, S.K. Multiobjective Evolution of Fuzzy Rough Neural Network via Distributed Parallelism for Stock Prediction. *IEEE Trans. Fuzzy Syst.* **2020**, *28*, 939–952. [CrossRef]
25. Fu, X.; Wu, X.; Zhang, C.; Fan, S.; Liu, N. Planning of Distributed Renewable Energy Systems under Uncertainty Based on Statistical Machine Learning. *Prot. Control Mod. Power Syst.* **2022**, *7*, 41. [CrossRef]
26. Stennikov, V.; Barakhtenko, E.; Mayorov, G.; Sokolov, D.; Zhou, B. Coordinated Management of Centralized and Distributed Generation in an Integrated Energy System Using a Multi-Agent Approach. *Appl. Energy* **2022**, *309*, 118487. [CrossRef]
27. León, L.F.; Martinez, M.; Ontiveros, L.J.; Mercado, P.E. Devices and Control Strategies for Voltage Regulation under Influence of Photovoltaic Distributed Generation. A Review. *IEEE Lat. Am. Trans.* **2022**, *20*, 731–745. [CrossRef]
28. Zhang, Z.; Zuo, Z.; Wang, Y. Distributed Control for State-of-Charge Balance and Load Voltage Regulation in DC Microgrids with Clustered Generations. *Asian J. Control* **2022**, *24*, 3456–3465. [CrossRef]
29. Pothireddy, K.M.R.; Vuddanti, S.; Salkuti, S.R. Impact of Demand Response on Optimal Sizing of Distributed Generation and Customer Tariff. *Energies* **2022**, *15*, 190. [CrossRef]
30. Yang, C.; Zou, X. Optimization Algorithm to Eliminate Solitary Point in the Tree Network. In Proceedings of the 2013 International Conference on Computational and Information Sciences, Shiyang, China, 21–23 June 2013; pp. 702–704. [CrossRef]
31. Lagace, P.J.; Vuong, M.H.; Kamwa, I. Improving Power Flow Convergence by Newton Raphson with a Levenberg-Marquardt Method. In Proceedings of the 2008 IEEE Power and Energy Society General Meeting—Conversion and Delivery of Electrical Energy in the 21st Century, Pittsburgh, PA, USA, 20–24 July 2008; pp. 1–6. [CrossRef]